Research papers

Coupled organic and inorganic carbon cycling in the deep subseafloor sediment of the northeastern Bering Sea Slope (IODP Exp. 323)

Laura M. Wehrmann [a,*], Nils Risgaard-Petersen [b], Heather N. Schrum [c,1], Emily A. Walsh [c], Youngsook Huh [d], Minoru Ikehara [e], Catherine Pierre [f], Steven D'Hondt [c], Timothy G. Ferdelman [a], Ana Christina Ravelo [g], Kozo Takahashi [h], Carlos Alvarez Zarikian [i] and The Integrated Ocean Drilling Program Expedition 323 Scientific Party [2]

[a] Department of Biogeochemistry, Max Planck Institute for Marine Microbiology, Celsiusstrasse 1, D-28359 Bremen, Germany
[b] Center for Geomicrobiology, Institute of Biological Sciences, Aarhus Universitet, Ny Munkegade Building 1540, 8000 Aarhus C, Denmark
[c] Graduate School of Oceanography, University of Rhode Island, South Ferry Road, Narragansett, RI 02882, USA
[d] School of Earth and Environmental Sciences, Seoul National University, Sillim-dong, Gwanak-gu, Seoul 151–747, Republic of Korea
[e] Center for Advanced Marine Core Research, Kochi University, B200 Monobe, Nankoku, Kochi 783–8502, Japan
[f] Laboratoire d'Océanographie Dynamique et de Climatologie (UMR 7159), Université Pierre et Marie Curie, 4 Place Jussieu, Case Courrier 100, 75252 Paris, France
[g] Ocean Sciences Department, University of California, 1156 High Street, Santa Cruz, CA 95064, USA
[h] Department of Earth and Planetary Sciences, Kyushu University, Hakozaki 6-10-1, Higashi-ku, Fukuoka 812–8581, Japan
[i] Integrated Ocean Drilling Program, Texas A&M University, 1000 Discovery Drive, College Station, TX 77845–9547, USA

ARTICLE INFO

ABSTRACT

We studied microbially mediated diagenetic processes driven by carbon mineralization in subseafloor sediment of the northeastern Bering Sea Slope to a depth of 745 meters below seafloor (mbsf). Sites U1343, U1344 and U1345 were drilled during Integrated Ocean Drilling Program (IODP) Expedition 323 at water depths of 1008 to 3172 m. They are situated in the high productivity "Green Belt" region, with organic carbon burial rates typical of the high-productivity upwelling domains on western continental margins. The three sites show strong geochemical similarities. The downward sequence of microbially mediated processes in the sediment encompasses (1) organoclastic sulfate reduction, (2) anaerobic oxidation of methane (AOM) coupled to sulfate reduction, and (3) methanogenesis. The sediment contains two distinct zones of diagenetic carbonate formation, located at the sulfate–methane transition zone (SMTZ) and between 300 and 400 mbsf. The SMTZ at the three sites is located between 6 and 9 mbsf. The upward methane fluxes into the SMTZ are similar to fluxes in SMTZs underlying high-productivity surface waters off Chile and Namibia. Our Bering Sea results show that intense organic carbon mineralization drives high ammonium and dissolved inorganic carbon (DIC) production rates (>4.2 mmol m^{-3} y^{-1}) in the uppermost 10 mbsf and strongly imprints on the stable carbon isotope composition of DIC, driving it to a minimum value of -27‰ (VPDB) at the SMTZ. Pore-water calcium and magnesium profiles demonstrate formation of diagenetic Mg-rich calcite in the SMTZ. Below the SMTZ, methanogenesis results in ^{13}C-enrichment of pore-water DIC, with a maximum value of $+11.9$‰. The imprint of methanogenesis on the DIC carbon isotope composition is evident down to a depth of 150 mbsf. Below this depth, slow or absent microbially mediated carbon mineralization leaves DIC isotope composition unaffected. Ongoing carbonate formation between 300 and 400 mbsf strongly influences pore-water DIC and magnesium concentration profiles. The linked succession of organic carbon mineralization and carbonate dissolution and precipitation patterns that we observe in the Bering Sea Slope sediment may be representative of passive continental margin settings in high-productivity areas of the world's ocean.

© 2011 Elsevier B.V. All rights reserved.

* Corresponding author. Tel.: +49 421 2028 655; fax: +49 421 2028 690.
E-mail addresses: lwehrman@mpi-bremen.de (L.M. Wehrmann), nils.risgaard-petersen@biology.au.dk (N. Risgaard-Petersen), hschrum@gso.uri.edu (H.N. Schrum), ewalsh@gso.uri.edu (E.A. Walsh), yhuh@snu.ac.kr (Y. Huh), ikehara@kochi-u.ac.jp (M. Ikehara), catherine.pierre@locean-ipsl.upmc.fr (C. Pierre), dhondt@gso.uri.edu (S. D'Hondt), tferdelm@mpi-bremen.de (T.G. Ferdelman), acr@pmc.ucsc.edu (A.C. Ravelo), kozo@geo.kyushu-u.ac.jp (K. Takahashi), zarikian@iodp.tamu.edu (C.A. Zarikian).
[1] Present address: Sea Education Association, P.O. Box 6, Woods Hole, MA 02543, USA.
[2] The IODP Expedition 323 Scientific Shipboard party members are: Ivano Aiello, Hirofumi Asahi, Gretta Bartoli, Beth Caissie, Muhong Chen, Elena Colmenero-Hidalgo, Mea Cook, Kelsie Dadd, Gilles Guèrin, Katrine Husum, Akira Iijri, Sev Kender, Douglas LaVigne, Tanzhuo Liu, Steve Lund, Christian März, Alan Mix, Maheswar Ojha, Makoto Okada, Yusuke Okazaki, Jonataro Onodera, Taoufik Radi, Tatsuhiko Sakamoto, David Scholl, and Zuzanna N. Stroynowski.

1. Introduction

The Bering Sea is regarded as a region of effective carbon sequestration, due to its highly efficient biological pump involving high biogenic opal fluxes, especially along the Bering Sea Slope (Takahashi, 1998, 1999). Sediment collected from the northeastern Bering Sea Slope affords an opportunity to study the fate of buried organic carbon associated with microbially mediated processes in the subsurface sediment of a very high productivity region. In particular, this deep sediment represents an excellent environment to evaluate biogeochemical processes and diagenetic carbon mineralization in a passive continental margin setting. In this setting, upward-migrating fluids from underlying seawater and brine reservoirs do not interrupt the succession of diagenetic processes associated with carbon burial, as often observed at active continental margins (e.g., Ocean Drilling Program (ODP) Leg 201 (D'Hondt et al., 2004)).

Microbially mediated processes significantly affect the subseafloor carbon cycle in the following ways. (1) Organic matter break-down and subsequent terminal electron accepting processes (TEAP), such as organoclastic sulfate reduction, affect pore-water pH, and thus, the saturation state of sedimentary carbonate phases. The reaction byproduct bicarbonate takes part in diagenetic carbonate formation (e.g., Ben-Yaakov, 1973; Boudreau and Canfield, 1988; Soetaert et al., 2007; Jourabchi et al., 2008). (2) During hydrogenotrophic and acetoclastic methanogenesis, hydrogen and acetate deriving from hydrolysis and fermentation of organic matter are utilized, and carbon dioxide (CO_2) and methane (CH_4) are produced (Martens and Berner, 1974; Sansone and Martens, 1981; Whiticar et al., 1986; Ferry, 1992; Whiticar, 1999):

$$CO_2 + 4H_2 \rightarrow CH_4 + 2H_2O \qquad (R1)$$

$$CH_3COOH \rightarrow CO_2 + CH_4 \qquad (R2)$$

Dissolved inorganic carbon (DIC) consumed during hydrogenotrophic methanogenesis originates from production by TEAP. (3) The anaerobic oxidation of methane (AOM) coupled to sulfate reduction consumes methane, and releases bicarbonate. This process, following the net reaction (Boetius et al., 2000; Hoehler et al., 1994; Valentine and Reeburgh, 2000; and reference therein),

$$CH_4 + SO_4^{2-} \rightarrow HCO_3^- + HS^- + H_2O \qquad (R3)$$

facilitates authigenic carbonate formation (e.g., Aloisi et al., 2002; Luff and Wallmann, 2003; Moore et al., 2004; Ussler and Paull, 2008).

Carbon cycling in subsurface sediment (>1.5 m sediment depth) is mediated by an active microbial community (D'Hondt et al., 2002, 2004; Parkes et al., 2005; Schippers et al., 2005; Jørgensen et al., 2006). Few studies have investigated the linkages between organic carbon mineralization, methane oxidation and diagenetic carbonate formation in the subseafloor biosphere (e.g., Kelts and McKenzie, 1982; Moore et al., 2004; Meister et al., 2007), particularly below the depth of sulfate depletion.

In this study, we present high-resolution measurements of several chemical properties at three sites on the Bering Sea Slope drilled to >700 meters below the seafloor (mbsf) by Integrated Ocean Drilling Program (IODP) Expedition 323. These data include dissolved chemical concentrations (dissolved inorganic carbon (DIC), sulfate, ammonium, calcium, magnesium, methane), solid-phase chemical concentrations (total organic carbon (TOC) and total inorganic carbon (TIC)), and the stable carbon isotope composition of DIC. These data, integrated with physical property data, allow us to calculate reaction rates and fluxes of pore-water constituents. We discuss the sequence of biogeochemical processes in the sediment with special focus on the extent of biologically catalyzed organic matter mineralization and its linkage to sedimentary inorganic carbon cycling. We examine microbially mediated processes and the fate of reaction byproducts such as DIC, throughout the sediment column.

2. Background

2.1. Study area

The Bering Sea marks the northernmost part of the Pacific Ocean. It is enclosed by the Alaskan Peninsula to the east and northeast, the Aleutian Archipelago to the south, and the Russian mainland and Kamchatka Peninsula to the west (Fig. 1). Its area is equally divided into a deep basin to the west and a large continental shelf (>500,000 km^2) that covers the eastern part of the Bering Sea. Present-day water circulation in the Bering Sea follows a cyclonic gyre fed by the Alaskan Coastal Current (ACC) and the Alaskan Stream, which enter northward through the Aleutian Islands (Reed, 1990; Stabeno et al., 2002; Ladd and Stabeno, 2009). The Alaskan Stream extends into the Bering Slope Current (BSC), which flows northeastward along the eastern Bering Sea Shelf and represents the eastern boundary current of the Bering Sea Gyre (Stabeno et al., 1999, 2009; Johnson et al., 2004).

These hydrodynamic conditions are integral to the existence of the Bering Sea Green Belt, a band of very high biological productivity along the continental shelf break, which is among the world's most productive oceanic regions (see Kinder and Coachman (1978); Okkonen et al. (2004); Springer et al. (1996); for review). Productivity in the Green Belt is sustained by the BSC, which delivers nitrate-rich deep waters to the photic zone. Macronutrients are also provided by surface waters from the Bering Sea basin to the west, and dissolved iron is delivered from bottom waters of the outer shelf (Aguilar-Islas et al., 2007). Estimates of annual primary production in the Green Belt are >170 g C m^{-2} y^{-1} (Hansell et al., 1993; Sambrotto et al., 2008). The high productivity of the Green Belt is in contrast to large areas of the open Bering Sea, which show characteristics of a High-Nutrient-Low-Chlorophyll (HNLC) region, and the Bering Sea Shelf, which is described as a nitrate-limited, iron-replete system (Banse and English, 1999; Moore et al., 2002; Tyrrell et al., 2005; Aguilar-Islas et al., 2007; Sambrotto et al., 2008).

2.2. Study sites and sediment composition

We present results from three sites drilled during IODP Expedition 323 along the northeastern Bering Sea Continental Slope in the Bering/Arctic Gateway region. This area is influenced by the Green Belt (Fig. 1). Sites U1343 and U1344 were cored to 745 mbsf and Site U1345 was cored to 150 mbsf. The seafloor of Site U1343 is located at 1952 m below sealevel (mbsl). Its sediment consists of alternating siliciclastic-rich and mixed siliciclastic-biogenic (diatom-bearing to diatom-rich) lithologies. Sedimentation rates at Site U1343 range from 21 to 58 cm ky^{-1}. Site U1344 is located at 3172 mbsl. Its sediment is silt with varying amounts of sand, clay, and diatoms and minor amounts of ash, foraminifers, nannofossils, and sponge spicules. Sedimentation rates range from 29 to 89 cm ky^{-1}. The water depth of Site U1345 is 1008 mbsl. Its sediment is siliciclastic with varying amounts of diatoms and minor amounts of foraminifers and calcareous nannofossils. This site has a mean sedimentation rate of ~28 cm ky^{-1}. Cored sediment at Sites U1343 and U1344 spans the early Pleistocene to Holocene. Sediment at Site U1345 was deposited from the middle Pleistocene to the Holocene (Expedition 323 Scientists, 2010).

3. Methods

3.1. Sample acquisition and processing

Sample acquisition and analyses of solid-phase, pore-water and hydrocarbon gas during IODP Expedition 323 followed standard
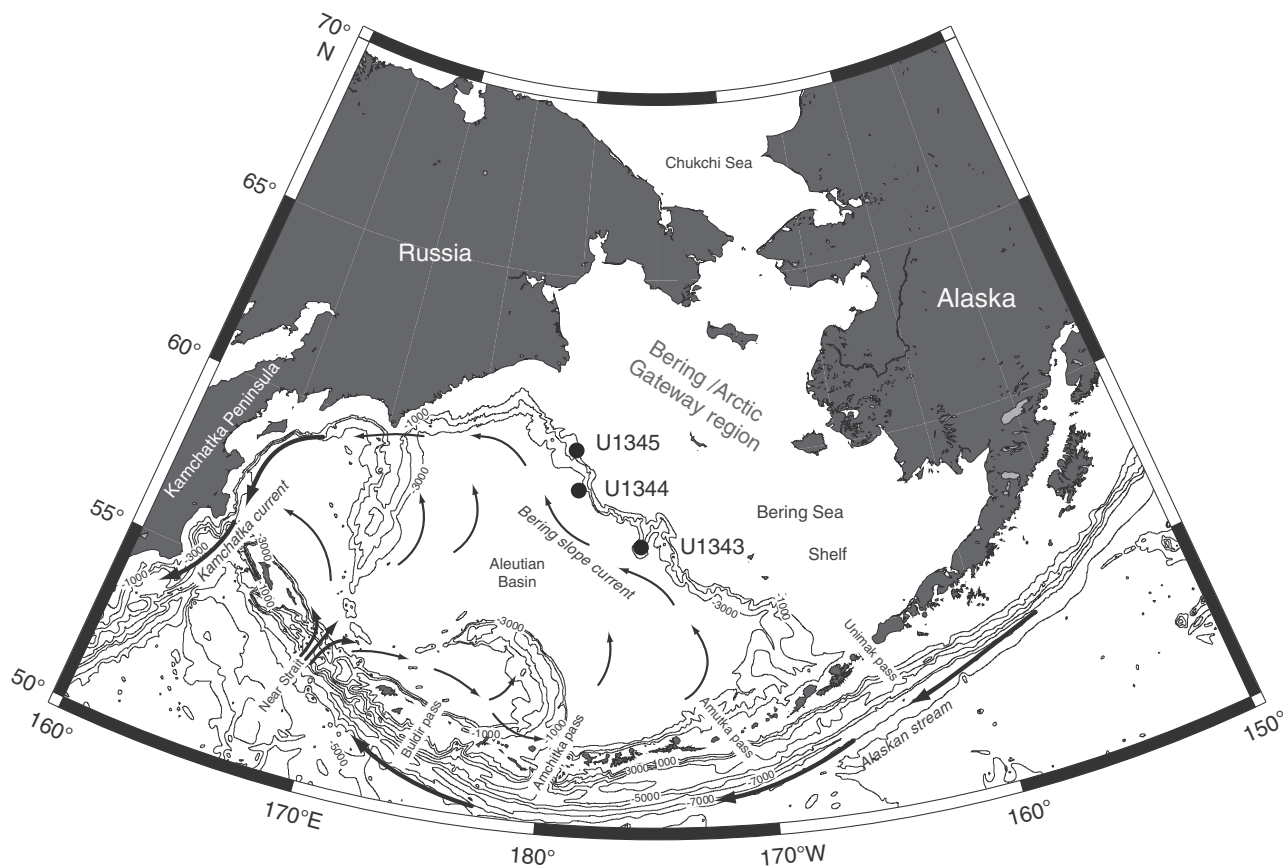
Fig. 1. Map of the Bering Sea with the three sites drilled during Integrated Ocean Drilling Program (IODP) Expedition 323 presented in this study. The sites are marked by filled circles. Black arrows indicate the present-day mean surface water circulation.

ODP protocols (Gieskes et al., 1991; Pimmel and Claypool, 2001). All sediment depths in this study are reported in corrected core composite depth below seafloor (CCSF-B) reported in meters below seafloor (mbsf). The CCSF-B depth scale corrects for effects of core expansion and incomplete core recovery, so the length of the cored section is the same as the drilled depth. Hence, it allows for measurements from multiple holes to be used on a common depth scale, and provides an accurate depth scale for absolute calculations of sedimentation rates and fluxes (Mix et al., 2003). The top 8 mbsf of the sediment at Site U1343 and the top 12 mbsf at Sites U1344 and U1345 were sampled at 25-cm intervals. The sampling interval was increased to between 70 cm and 150 cm down to a depth of ~34 mbsf at all three sites. At greater depth, one sample was taken every core (at ~9.5 m intervals), except for the interval deeper than 370 mbsf at Site U1344, where one sample was taken every other core. Pore-water was extracted from whole rounds using a Manheim-type hydraulic press (Manheim et al., 1994). Whole-round squeeze cakes were used for solid-phase analyses. Dissolved inorganic carbon (DIC) was measured using a UIC 5011 CO_2 coulometer. Sulfate, calcium, and magnesium concentrations were determined with a Dionex ICS-3000 ion chromatograph. Ammonium concentrations were determined spectrophotometrically (Shimazu UV mini 1240 UV-Vis spectrophotometer), based on the method of Solórzano (1969). Total carbon (TC) content was determined using a Thermo Electron Flash EA 1112 Element Analyzer. Total inorganic carbon (TIC) content was determined with a UIC 5011 CO_2 coulometer. Total organic carbon (TOC) was calculated as the difference between TC and TIC. Coefficients of variation for dissolved chemical concentrations except ammonium

and for solid-phase measurements were <2%. The coefficient of variation for ammonium analyses was 0.5%.

Stable carbon isotope composition of DIC was determined on a Gasbench II (Thermo) coupled to a DELTA V plus IRMS (Thermo), according the method of Torres et al. (2005). The DIC carbon isotope composition is reported in delta notation relative to Vienna Pee Dee Belemnite Standard (VPDB), on a scale normalized by assigning consensus values of −46.6‰ to the reference material L-SVEC lithium carbonate and +1.95‰ to the reference material NBS-19 calcium carbonate (Coplen et al., 2006). Both materials were used as internal standards during the analysis. The standard error (1σ) of the measurement was less than 0.05‰ for $\delta^{13}C$.

At Site U1343, samples for hydrocarbon gas analyses were taken only after core transport and opening in the cold lab. At Sites U1344 and U1345, high-resolution sampling for hydrocarbon gas analyses in the uppermost 15 mbsf took place on the catwalk of the *JOIDES Resolution*. For Site U1345, the dissolved methane profile is smooth across the SMTZ and above (Fig. 2), indicating that *in situ* gas concentrations were below sea-surface saturation concentrations. The noisy profiles just below the SMTZ at Sites U1343 and U1344 and for greater depths at all three sites suggest that cores from deeper strata lost significant gas during core recovery, because the gas content exceeded the sea saturation concentration under sea-surface conditions. For this reason, methane data from Sites U1343 and U1344 were excluded from numerical modeling. Solid-phase as well as pore-water shipboard data will be available in the DSDP/ODP/IODP Janus data base and in the IODP Expedition 323 proceedings. The DIC carbon isotope composition for all three sites is presented in Table S1 as supplementary material to this manuscript.
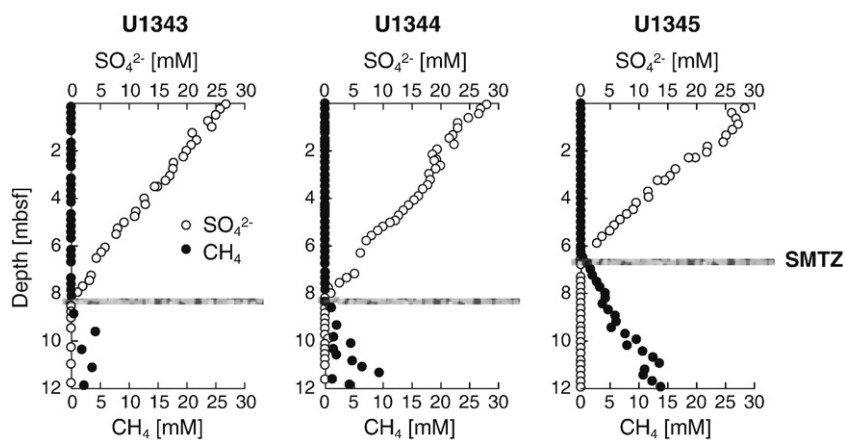
Fig. 2. Pore-water sulfate (SO_4^{2-}) and methane (CH_4) concentrations with depth for the top 12 m of the sediment column at Sites U1343, U1344, and U1345. The grey bars show the inferred depths of the sulfate-methane transition zones (SMTZ).

3.2. Flux and reaction rates

We calculated fluxes of DIC, methane, sulfate, calcium, and magnesium using Fick's First Law,

$$J = -\phi D_s \frac{\partial C}{\partial x}, \qquad (1)$$

where J is flux, ϕ is measured porosity, D_s is the temperature-corrected bulk sediment diffusion coefficient, and $\frac{\partial C}{\partial x}$ is the vertical gradient of the dissolved constituent (Berner, 1980). D_s was calculated from $D_s = D_o \phi_{avg}^2$, where D_o is the free diffusion coefficient in water (Ullman and Aller, 1982; Boudreau, 1997). By executing the program PROFILE (Berg et al., 1998), rates of reaction were quantified for DIC and ammonium using numerical solutions to the one-dimensional mass conservation equation,

$$\frac{d}{dx}\left(\phi(D_s + D_B)\frac{dC}{dx}\right) + \phi\alpha(C_o - C) + R = 0, \qquad (2)$$

where D_B is temperature-corrected biodiffusivity, C is the pore-fluid solute (DIC or ammonium) concentration, C_o is the bottom-water solute concentration, x is depth, α is the irrigation coefficient, and R is the net rate of production (or consumption if R is negative) of DIC or ammonium per unit volume of sediment (Berg et al., 1998). D_B was used to correct for temperature dependency of molecular diffusion as the program PROFILE only allows for a fixed value for D_s/ϕ^2 (P. Berg, pers. comm.). Temperature correction is based on measured geothermal gradients of 49.0 °C km^{-1} at Site U1343 and 48.5 °C km^{-1} at Site U1345 (Expedition 323 Scientists, 2010). We assumed no irrigation (i.e. $\alpha = 0$) and steady state conditions for all concentration profiles. Pore-water profiles from Site U1344 revealed variation in the concentration of the measured pore-water constituents that could not be resolved by this modeling procedure. Consequently, this site was excluded from geochemical modeling. Based on our modeling results for DIC, which show that main DIC production is confined to the top 70 m of the sediment, we distinguish between the processes occurring in the top 70 mbsf and the deeper sediment layers in the results and discussion section.

The organic carbon burial rate for the last 0.3 Ma at all three sites was calculated using average sedimentation rates, wet bulk density, porosity and total organic carbon content. Sediment age was determined from the average last occurrence of *Spongodiscus* sp. at each site (Expedition 323 Scientists, 2010).

3.3. Ion activity product (IAP) of dolomite

The ion activity product (IAP) for dolomite at Sites U1343 and U1344 was calculated using an approach similar to Moore et al. (2004). The pore-water CO_3^{2-} concentration was determined from the pore-water calcium concentration, assuming equilibrium between the solid-phase calcite and pore-water CO_3^{2-}, using a log $K_{sp\text{-}calcite}$ of -8.48. The log IAP of dolomite was then established from the calculated value for $[CO_3^{2-}]$ and the pore-water magnesium and calcium concentrations, assuming that concentrations equal ion activity for depths below the SMTZ (Moore et al., 2004). The calculated values for the log IAP of dolomite for Sites U1343 and U1344 are presented in Table S1 as supplementary material to this manuscript.

4. Results and discussion

4.1. Biogeochemical processes at the sulfate-methane transition zone (SMTZ)

Pore-water sulfate concentration profiles from Sites U1343, U1344, and U1345 exhibit a near-linear decrease in the top 6 to 9 mbsf, accompanied by an increase in methane concentration at the depth of sulfate depletion (Figs. 2 and 3). In ocean-margin sediment, sulfate reduction coupled to AOM leads to the formation of a SMTZ in the top meters of the sediment column (D'Hondt et al., 2002). At the Bering Sea sites, the upward diffusing methane is provided by methanogenesis in deeper sediment rather than by a deep (thermogenic) reservoir, as these sites show predominately biogenic hydrocarbon ratios, with a methane/ethane ratio of >10,000 (Expedition 323 Scientists, 2010). As at other high-productivity continental margins, burial of organic carbon at these sites is sufficient to sustain high microbial metabolic activity driving sulfate depletion and the onset of methanogenesis (see Mitterer (2010); for review).

High-resolution pore-water data from Site U1345 allow us to constrain biogeochemical fluxes associated with the SMTZ (Fig. 3). The calculated downward sulfate and upward methane fluxes into the SMTZ do not follow a 1:1 stoichiometry, which would theoretically be expected based on Reaction R3. The methane flux accounts for only 77% of the sulfate flux into the SMTZ. This difference between sulfate and methane fluxes can be attributed to either 1) methane loss during core recovery and sample processing leading to underestimation of methane concentrations at depth (Paull et al., 2000), or 2) organoclastic sulfate reduction impinging on the pore-water sulfate concentration profile (Kastner et al., 2008).
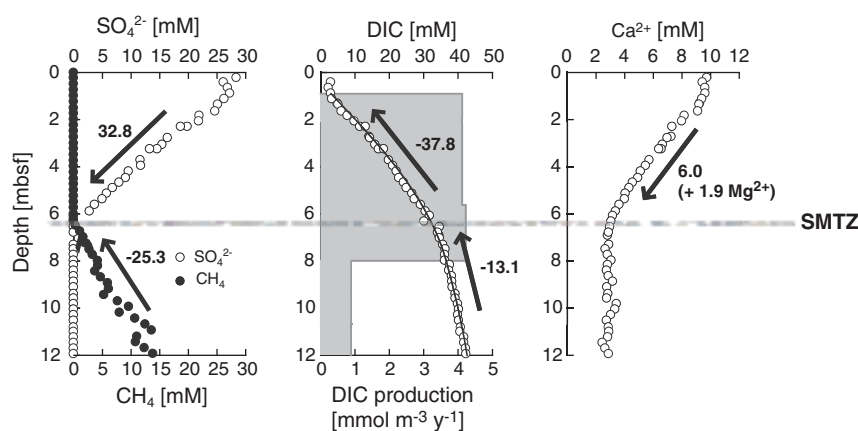
Fig. 3. Pore-water sulfate (SO_4^{2-}) and methane (CH_4) concentrations, dissolved inorganic carbon (DIC) concentration and production rate (grey bars), and calcium concentration at Site U1345. Also shown are the fluxes of the pore-water constituents across the SMTZ; negative values denote upward fluxes. All fluxes are given in mmol m^{-2} y^{-1}.

To assess these alternatives, we calculated carbon mass balance, based on the fluxes of DIC across the SMTZ and taking into account DIC removal by authigenic carbonate formation. Similar approaches have been used by Snyder et al. (2007) and Wehrmann et al. (2009). Our mass balance calculation shows that some methane was probably lost during coring and sampling procedures.

The net change of DIC across the SMTZ ($\Delta_{DIC-Prod}$) is calculated as:

$$\Delta_{DIC-Prod} = F_{DIC-Shallow} - F_{DIC-Deep} - F_{Carb} \qquad (3)$$

where $F_{DIC-Shallow}$ is the (upward) flux of DIC above the SMTZ, $F_{DIC-Deep}$ is the (upward) flux of DIC into the SMTZ, and F_{Carb} is the sum of the downward fluxes of calcium (F_{Ca}) and magnesium (F_{Mg}). This calculation gives a value for Δ_{DIC} of -32.6 mmol m^{-2} y^{-1} based on the fluxes displayed in Fig. 3. This value is in good agreement with the calculated flux of sulfate into the SMTZ of 32.8 mmol m^{-2} y^{-1}, because the change of DIC across the SMTZ ($\Delta_{DIC-Prod}$) equals the flux of sulfate into the SMTZ (F_{SO4}) if sulfate reduction coupled to AOM is the dominating process removing sulfate, thus producing DIC in a 1:1 stoichiometry.

We compare the upward methane fluxes into the SMTZ at Site U1345 to fluxes determined for ODP Leg 201 Site 1227 (Biddle et al., 2006) and Station GeoB 7186 (Treude et al., 2005), which underlie high-productivity surface water along the Peruvian and Chilean shelf, and Station GeoB 3718, which underlies Namibian upwelling on the African continental slope (Niewöhner et al., 1998) (Table 2). The methane fluxes at the Bering Sea Slope sites are well within the range of fluxes determined for these mid- to low-latitude high-productivity upwelling areas. Notably, the methane fluxes are one to two orders of magnitude lower than methane fluxes determined for active continental margin settings where methane ascends from deep biogenic and thermogenic methane sources by advective transport, e.g., Hydrate Ridge (8690 mmol m^{-2} y^{-1}; Luff and Wallmann, 2003). Nonetheless, given that methane at the Bering Sea Slope sites is predominately of biogenic origin, our results highlight the importance of methanogenesis in the deep biosphere of high primary productivity regions.

4.2. Organic matter mineralization

Pore-water ammonium and DIC concentration profiles from Sites U1343, U1344, and U1345 reflect high rates of microbially mediated organic carbon degradation. Ammonium is among the best indicators for the magnitude of organic matter degradation because only a limited number of processes consume dissolved ammonium in subsurface sediment. Ammonium can be removed from solution by adsorption onto mineral particles (Müller, 1977; Mackin and Aller, 1984). This process is less important in aged compared to fresh marine sediment (Hensen and Wallmann, 2005). Recent geochemical evidence suggests that it may also be removed by sulfate-reducing ammonium oxidation (Schrum et al., 2009). At Sites U1344 and U1345, ammonium increases from low values near the sediment–water interface to an interval where the concentration gradients are minimal, followed by a pronounced increase very close to the depth where sulfate concentrations approach zero, suggesting that sulfate-reducing ammonium oxidation may be a sink for ammonium at some Bering Sea sites.

More specifically, ammonium concentrations at Sites U1343 and U1344 increase with depth from 0.09 mM near the sediment–water interface to maximum values of 13.3 mM at 570 mbsf and 11.6 mM at 660 mbsf depth, respectively (Figs. 4a and b). At Site U1345, ammonium concentrations increase throughout the sediment column to a maximum value of 9.1 mM at 139 mbsf (Fig. 4). At Sites U1343 and U1345, high rates of ammonium production are confined to the uppermost 10 mbsf of sediment, with maximum production rates in the top 3.1 m and 5.5 mbsf (Fig. 4a and c), respectively. At Site U1343, ammonium production rates of ~0.014 mmol m^{-3} y^{-1} occur from 10 to 30 mbsf, below which rates decrease by one order of magnitude. Similarly, ammonium production rates at Site U1345 indicate a sharp decrease in production to rates <0.01 mmol m^{-3} y^{-1} below 10 mbsf. The downward decreases in ammonium production rates can be attributed to decreasing consumption of organic matter, as organic concentration and organic matter reactivity decrease with increasing sediment age (Middelburg, 1989; Boudreau and Ruddick, 1991).

Table 1
Site location, water depth, average sedimentation rate for the last 0.3 Ma, organic carbon burial rates, the present depth of the sulfate-methane transition zone (SMTZ), and the approximate bottom water oxygen (O_2) concentration (*based on Garcia et al. (2006)) for the three investigated sites.

Site	Location	Water depth [mbsl]	Average sedimentation rate for last 0.3 Ma [cm ky^{-1}]	Organic carbon burial rate [mmol m^{-2} y^{-1}]	Present depth of SMTZ [mbsf]	Approx. bottom water O_2 concentration* [μmol]
U1343	57°33.4156′N/175°48.9951′W	1952	29	171	~8.3	~65.9
U1344	59°3.0005′N/179°12.2011′W	3172	41	251	~8.1	~89.3
U1345	60°9.2003′N/179°28.2127′W	1008	28	199	~6.3	OMZ

Table 2
Water depth, present depth of the SMTZ and upward flux of methane (CH_4) into the SMTZ at Site U1345, ODP Leg 201 Site 1227 (Biddle et al., 2006), Station GeoB 7186 (Treude et al., 2005), and Station GeoB 3718 (Niewöhner et al., 1998).

Site	Location	Water depth [mbsl]	Present depth of SMTZ [mbsf]	Upward flux of CH_4 into the SMTZ [mmol m^{-2} y^{-1}]
U1345	Bering Sea Slope	1020	~6.3	25.3
1227	Peruvian shelf	427	~40	16
GeoB 7186	Chilean continental margin	1168	2.9	25.4
GeoB 3718	Namibian continental slope	1312	~6	30.2

Total organic carbon (TOC) contents at Sites U1343, U1344, and U1345 are mostly between 0.5% and 1% (Fig. 4). Organic carbon burial rates at the three sites range from 171 to 251 mmol m^{-2} y^{-1} (Table 1). These rates are very similar to rates determined for the Namibian upwelling region (~250 mmol m^{-2} y^{-1}; Berger and Wefer, 2002) and ODP Sites 1227 and 1230 drilled on the Peru Margin (310 mmol m^{-2} y^{-1}; D'Hondt et al., 2004).

Site U1343 is characterized by the lowest organic carbon burial rate of the three sites, followed by Site U1345. Site U1344 has both the highest sedimentation rate and the highest organic carbon burial rate. Although its organic burial rate is less than at Site U1344, Site U1345 has the shallowest SMTZ and the highest DIC production rate, most likely because it underlies the water-column oxygen minimum zone (OMZ) (Table 1). Under low bottom-water oxygen conditions, organic matter buried in the underlying sediment gets less degraded, and a shift from aerobic to more anaerobic degradation pathways occurs (Canfield, 1994; Hedges and Keil, 1995; Hartnett and Devol, 2003; Middelburg and Levin, 2009; Vandewiele et al., 2009). The increased availability of easily degradable organic matter results in higher organoclastic sulfate reduction rates in the uppermost sediment, higher rates of methanogenesis, and, in a system dominated by biogenic methane, a higher upward methane flux at Site U1345. Elevated anaerobic oxidation rates in the topmost sediment zone at Site U1345 result in enhanced DIC production compared to Site U1343. The upward flux of methane is counterbalanced by the diffusive downward flux of sulfate from seawater. A higher flux of methane at Site U1345 compared to the other sites is indicated by its shallower SMTZ, because an increase in the sulfate flux is induced by a shoaling of the SMTZ (Moore et al., 2004; Sivan et al., 2007).

The finding that U1345, although not characterized by the highest organic carbon burial rate, has the shallowest SMTZ and highest DIC production rates suggests that the effect of the OMZ on the degradability of organic matter exerts a stronger control on the organic carbon oxidation rates (and ultimately the depth of the SMTZ) than the overall flux of organic carbon to the sediment at the investigated sites. Interestingly, the difference in the extent of organic carbon respiration at the three sites is less apparent below the SMTZ because geochemical profiles are very similar at Sites U1343 and U1344. Thus, the influence of the OMZ is most important during early stages of diagenesis while its signal may ultimately not reach the deep biosphere.

4.3. Transformations of the dissolved inorganic carbon (DIC) pool

4.3.1. Dissolved inorganic carbon distribution and carbon isotope composition in the top 70 m

The shape of the DIC concentration profiles and the DIC carbon isotope composition in the uppermost 70 mbsf of the sediment column at the three sites are typical for methane-bearing continental margin sediment (e.g., Luff and Wallmann, 2003; Wallmann et al., 2006; Snyder et al., 2007). Dissolved inorganic carbon concentrations strongly increase in the top 20 mbsf and reach maximum values of 59 to 74 mM (Fig. 5). This increase is driven by organic carbon oxidation with organoclastic sulfate reduction as the primary

TEAP, and sulfate reduction coupled to AOM at the SMTZ. The SMTZ often represents an inflection point in the profile due to enhanced DIC production during AOM (Snyder et al., 2007). At the Bering Sea Slope sites, this inflection point is not pronounced, presumably because of high DIC production during fermentation and organoclastic sulfate reduction above the SMTZ, as observed in elevated DIC production rates at shallow depth (Fig. 5). The DIC carbon isotope composition shows increasing depletion in ^{13}C in the uppermost 5.5 to 8.0 mbsf at all three sites with minimum values of −26.9‰, −24.0‰ and −25.5‰ at Sites U1343, U1344 and U1345 (Fig. 5), respectively. Minimum values coincide with the depth of sulfate depletion at the SMTZ. ^{13}C-depletion of the DIC can be attributed to carbon isotope fractionation during organic carbon mineralization by organoclastic sulfate reduction and, more importantly, during anaerobic oxidation of ^{13}C-depleted methane (McCorkle et al., 1985; Alperin et al., 1988; Martens et al., 1999).

Below the SMTZ, DIC production can be attributed to fermentation and subsequent methanogenesis. Both processes release CO_2 into the pore-water DIC pool. At the three sites, elevated ammonium production rates below the SMTZ (Fig. 4) indicate ongoing fermentation and production of labile organic compounds, such as acetate, which facilitate high rates of methanogenesis (Reactions R2 and R3). $\delta^{13}C$ values of DIC increase strongly from minimum values <−24‰ at the SMTZ to maximum values of +11.9‰ at 135 mbsf at Site U1343 and +11.4‰ at 143 mbsf at Site U1344. These values reflect the high rates of methanogenesis because this process results in the release of strongly ^{13}C-enriched CO_2 (Whiticar, 1999).

DIC production is highest in the uppermost 0 to 12 mbsf at U1343 (1.87 mmol m^{-3} y^{-1}) and 0 to 8 mbsf at U1345 (4.17 mmol m^{-3} y^{-1} (Fig. 5)). It is less pronounced in the immediately underlying sediment (12 to 30 mbsf and 8 to 33 mbsf, at U1343 and U1345 respectively). The decline of DIC production rates with depth can be attributed to the absence of AOM below the depth of the SMTZ, and a decline in organic matter reactivity, which controls rates of fermentation and methanogenesis below the SMTZ.

The pore-water calcium and magnesium profiles demonstrate ongoing carbonate formation in the SMTZ. Calcium concentration profiles at the three sites correlate well with sulfate concentration profiles and show an almost linear decrease from near-seawater values at the sediment surface to values of 2.9 to 3.5 mM at the depth of the SMTZ (Fig. 6). This decrease in calcium is accompanied by a subtle decrease in pore-water magnesium concentration (Fig. 6). This coincident decrease in calcium and magnesium concentrations suggests formation within the SMTZ of either (1) Mg-rich calcite or (2) simultaneous dolomite and calcite phases, as previously described for methane-bearing continental margin sediment (e.g., Kelts and McKenzie 1982; Meister et al. 2007; Ussler and Paull, 2008). Distinct diagenetic carbonate layers at the SMTZ are not observed in Bering Sea Slope sediment because persistent high sedimentation rates at these sites do not permit maintenance of the SMTZ at a fixed depth for enough time to precipitate well-developed diagenetic fronts (Ussler and Paull, 2008). Shallowest occurrences of diagenetic carbonate layers are at 37.1 mbsf at Site U1343, 52.7 mbsf at Site U1344 and at 43.0 mbsf at Site U1345.
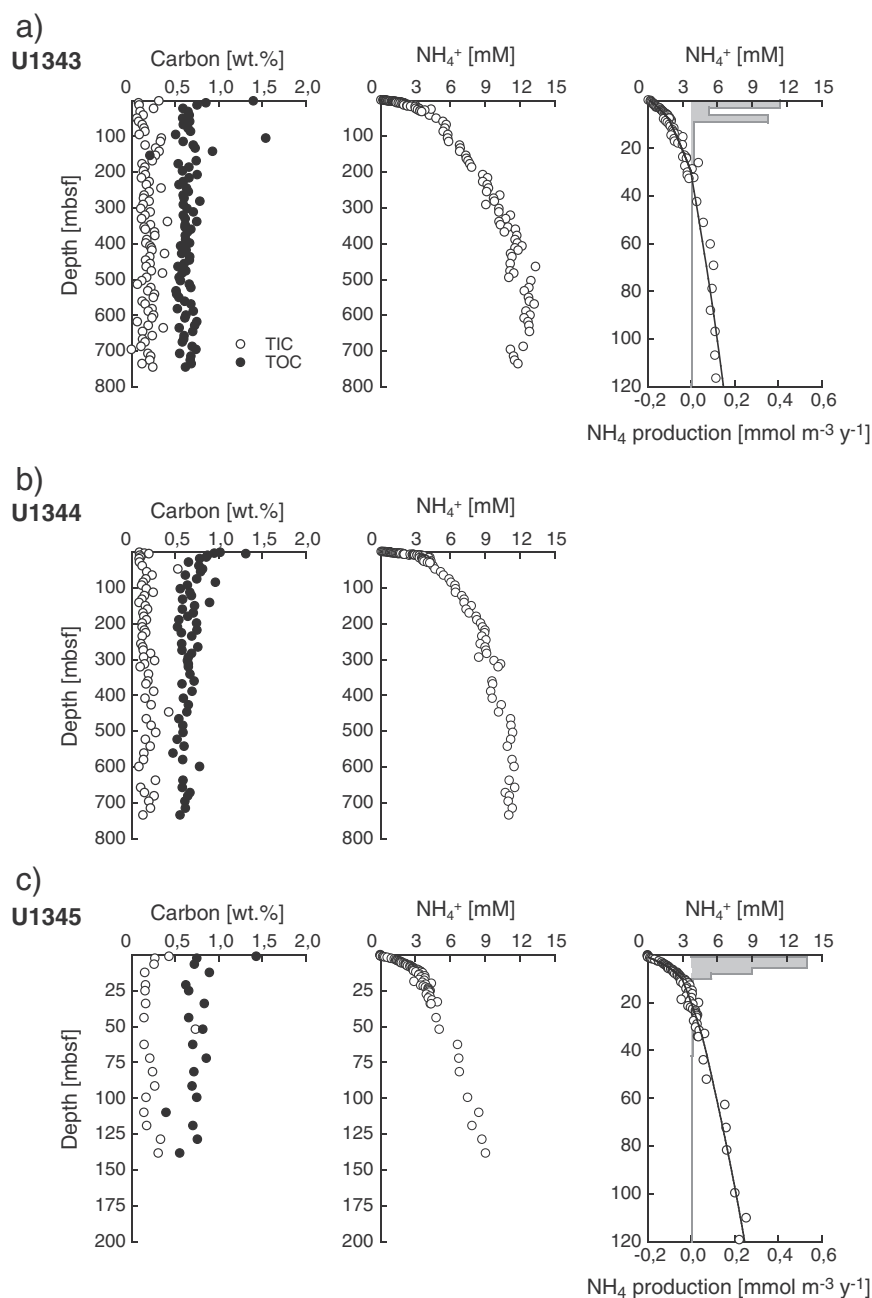
Fig. 4. Solid-phase total inorganic carbon (TIC) and organic carbon (TOC), pore-water ammonium (NH_4^+) concentrations with depth a) at Sites U1343, b) Site U1344 and c) Site U1345. Also shown are calculated least-square fit concentration profiles (black lines) and modeled rates of production (positive values) and consumption (negative values; grey bars) for pore-water ammonium concentration profiles for the top 120 m of Sites U1343 and U1345.

4.3.2. Dissolved inorganic carbon distribution and carbon isotope composition in the deep sediment (>70 m)

At Sites U1343 and U1344, DIC concentration profiles show a pronounced decrease below ~87 mbsf, with concentration minima at ~340 mbsf and ~390 mbsf, respectively (Fig. 5a and b). At Site U1343, net consumption of DIC is 0.02 mmol m^{-3} y^{-1} between 300 and 385 mbsf. Dissolved inorganic carbon consumption in the deep subseafloor at both sites can be attributed to a second zone of diagenetic carbonate formation. Subsurface formation of diagenetic carbonate has been previously described for several sites in high-productivity continental margin settings, with dolomite as the principal mineral formed ("organogenic dolomite"; see Compton (1988), Mazzullo (2000); for review). The formation of carbonate well within the methanogenic zone is most likely promoted by marine silicate weathering which converts CO$_2$ produced during organic

matter mineralization and carbonate formation at shallower depth, into bicarbonate (Wallmann et al., 2006, 2008). This process also releases magnesium and calcium ions into the pore-water which may be bound in the carbonate formation zone.

Near-linear magnesium profiles at these depths (Fig. 6a and b) are evidence that a Mg-rich carbonate such as dolomite is forming at ~340 mbsf and ~390 mbsf at Sites U1343 and U1344, respectively. In contrast, calcium concentrations are relatively constant with depth. The calcium required for carbonate formation probably derives from silicate mineral weathering but may also originate from *in situ* dissolution of previously formed diagenetic carbonate and biogenic carbonate phases (Baker and Burns, 1985; Compton and Siever, 1986; Compton, 1988).

To test whether the formation of dolomite is likely we calculated the log IAP of dolomite which ranges from −15.5 to −17.0 at Sites
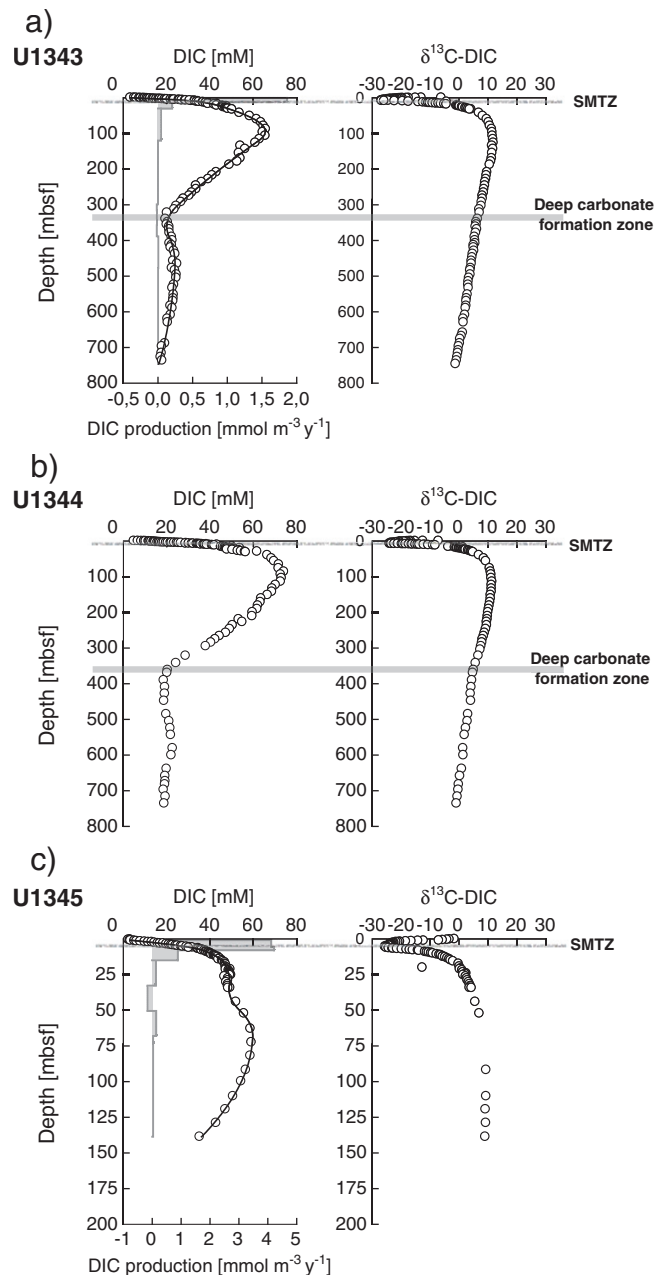
Fig. 5. Pore-water dissolved inorganic carbon (DIC) concentrations and stable carbon isotope composition of DIC (δ^{13}C-DIC) at a) Site U1343, b) Site U1344 and c) Site U1345. Shown are also calculated least-square fit concentration profiles (black lines) and modeled rates of production (positive values) and consumption (negative values; grey bars) for pore-water DIC concentration profiles of Sites U1343 and U1345. The grey bars show inferred depths of the SMTZ and the deep carbonate formation zone.

U1343 and U1344 (Fig. 6a and b, Table S1). At the assumed depths of dolomite formation, values are − 16.2 (Fig. 6), which agrees well with a log $K_{sp-dolomite}$ value of − 16.1 to − 16.4 proposed by Moore et al. (2004) based on pore-water data from sites drilled along the western African margin during ODP Leg 175. It needs to be noted, however, that the proposed range for the log $K_{sp-dolomite}$ by Moore et al. (2004) is rather narrow compared to previous estimates, e.g., of − 16.54 for disordered dolomite to − 19.71 for stoichiometric dolomite (Lippmann, 1973; Stumm and Morgan, 1996). It is nonetheless likely that dolomite is forming at the predicted depths of carbonate formation. Similar to other diffusive diagenetic interfaces, the carbonate formation zone probably moves upward through the sediment column during sediment burial (Berner, 1980; Burdige, 2006). Based on net DIC consumption in the

deep carbonate formation zone the rates of carbonate formation are very slow, and the amount of carbonate forming is small compared to the background sedimentary carbonate content. Nonetheless, these diagenetic carbonates represent an important sink for DIC in the deep subseafloor sediment. Below the carbonate formation zone at Sites U1343 and U1344, calcium concentrations decrease further while magnesium concentrations slightly increase. These profiles may be evidence of continued low rates of dolomitization of calcite phases in the deeply buried sediment.

At Site U1343, the depth of dolomite formation might be influenced by a lithological change. The predicted zone of carbonate formation is located a few meters above a distinct layer of stiff low-density clays. This interval could serve as a diffusional boundary layer and inhibit the downward migration of pore-water constituents. A similar lithological alteration was not observed at Site U1344 (Expedition 323 Scientists, 2010). A deep carbonate formation zone is probably also present at Site U1345 below the maximum coring depth, as DIC and magnesium concentration profiles from this site also show the characteristic decrease below ~75 mbsf (Figs. 5c and 6c).

The pore-water DIC profiles at Sites U1343 and U1344 are strongly controlled by the inferred carbonate formation zone at depth which acts as a DIC sink. DIC production, by fermentation and methanogenesis, does not appear to imprint the pore-water DIC concentration profile below 150 mbsf, although there is indication for subtle DIC production between 480 and 750 mbsf based on PROFILE modeling results (Fig. 5). Thus, at these depths, fermentation and methanogenesis occur only at extremely low rates or are entirely absent. Cessation of methanogenesis at depth has been previously described by Sivan et al. (2007) for deep sediment from the West African margin drilled during ODP Leg 175. They attributed the absence of methanogenesis below 200 mbsf to the decline of organic matter reactivity with depth. The authors also suggested alternatively that this absence might be due to a change in microbial community structure or an inhibitory effect of metabolic products (such as methane) on methanogenic activity at depth.

The carbon isotope composition of the pore-water DIC shows continued ^{13}C-enrichment at the three sites from 70 mbsf to ~150 mbsf, indicating ongoing low rates of methanogenesis in this depth range (Fig. 5). Below 150 mbsf, δ^{13}C values decrease gradually to − 1.1‰ and − 0.8‰ in the deepest sediment drilled at Sites U1343 and U1344, respectively (Fig. 5). The observed isotope distribution results from input of ^{13}C-depleted DIC, derived from (1) dissolution of biogenic calcite and diagenetic carbonate formed at shallow depth and (2) continuous exchange between pore-water carbonate and solid-phase carbonate.

5. Summary and conclusions

Our study shows that organic and inorganic carbon undergo major transformations during all stages of burial in the deep subseafloor sediment of the high-productivity Bering Sea. We observe a characteristic succession of microbially mediated diagenetic processes that alter sediment lithology, dissolved chemical profiles and the carbon isotope composition of DIC. Anaerobic carbon mineralization occurs in the top meters, most likely with organoclastic sulfate reduction as the main TEAP. Where upward diffusing methane and downward diffusing sulfate intercept, sulfate reduction coupled to AOM drives formation of Mg-rich calcite. Although upward diffusing methane primarily originates from methanogenesis proceeding at high rates below the SMTZ, methanogenic rates decline with depth. Below 150 mbsf, there is no evidence for methanogenesis in the pore-water DIC signal. The flux of methane into the SMTZ at Site U1345 is well within the range of fluxes determined for other sites in high-productivity upwelling areas, underlining the importance of methanogenesis during diagenesis in these continental margin settings.
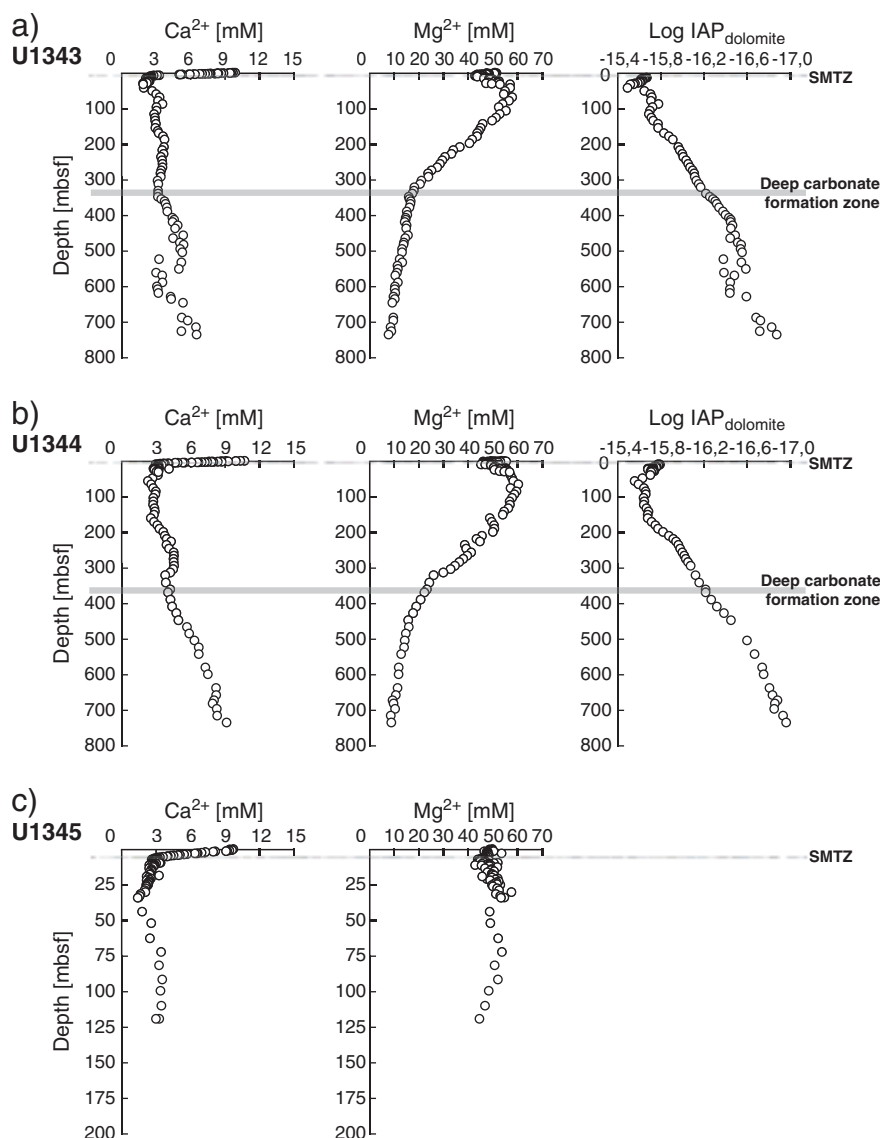
Fig. 6. Pore-water calcium (Ca^{2+}), and magnesium (Mg^{2+}) concentrations at a) Site U1343, b) Site U1344 and c) Site U1345 and the ion activity product (IAP) of dolomite with depth at a) Site U1343 and b) Site U1344. The grey bars show inferred depths of the SMTZ and the deep carbonate formation zone.

Organic carbon mineralization, methane oxidation, and methanogenesis are sources of DIC, which diffuses upward within the sediment and leaves a characteristic imprint on the carbon isotopic composition of the DIC. A deep zone of diagenetic carbonate formation strongly influences pore-water DIC and magnesium concentrations. We hypothesize that dolomite is precipitating in this zone. Calcium for carbonate precipitation in the deep carbonate formation zone derives from silicate weathering but may also constitute a fraction deriving from the dissolution and recrystallization of buried biogenic carbonate and diagenetic carbonate phases precipitated at shallow depth. Comparison to previous studies (e.g., Kelts and McKenzie, 1982; Moore et al., 2004) suggests that dolomite formation below the zone of methanogenesis (where the pore-water carbonate saturation state favors the formation of dolomite over calcite) may be a common process at high-productivity continental margins.

Subtle differences in the extent of organic carbon oxidation at the three sites probably result from differences in organic carbon burial rates and bottom water oxygen concentrations. These signals are most pronounced during early diagenesis. Strong geochemical similarities below the SMTZ at Sites U1343 to U1345 suggest that these inter-site differences do not significantly affect the succession of organic carbon mineralization and patterns of carbonate dissolution and precipitation at depth. The sequence of diagenetic processes and carbon sequestration that occurs in the Bering Sea Slope sediment may be representative of passive ocean-margin sediment underlying high-productivity surface waters throughout the world's ocean.

Supplementary materials related to this article can be found online at doi:10.1016/j.chemgeo.2011.03.002.

References

Aguilar-Islas, A.M., Hurst, M.P., Buck, K.N., Sohst, B., Smith, G.J., Lohan, M.C., Bruland, K.W., 2007. Micro- and macronutrients in the southeastern Bering Sea: insight into iron-replete and iron-depleted regimes. Prog. Oceanogr. 73, 99–126.

Aloisi, G., Bouloubassi, I., Heijs, S.K., Pancost, R.D., Pierre, C., Damsté, J.S.S., Gottschal, J.C., Forney, L.J., Rouchy, J.M., 2002. CH_4-consuming microorganisms and the formation of carbonate crusts at cold seeps. Earth Planet. Sci. Lett. 203, 195–203.

Alperin, M.J., Reeburgh, W.S., Whiticar, M.J., 1988. Carbon and hydrogen isotope fractionation resulting from anaerobic methane oxidation. Glob. Biogeochem. Cycles 2, 278–288.

Baker, P.A., Burns, S.J., 1985. Occurrence and formation of dolomite in organic-rich continental-margin sediments. AAPG Bull. 69, 1917–1930.

Banse, K., English, D.C., 1999. Comparing phytoplankton seasonality in the eastern and western subarctic Pacific and the western Bering Sea. Prog. Oceanogr. 43, 235–288.

Ben-Yaakov, S., 1973. pH buffering of pore water of recent anoxic marine sediments. Limnol. Oceanogr. 18, 86–94.

Berg, P., Risgaard-Petersen, N., Rysgaard, S., 1998. Interpretation of measured concentration profiles in sediment pore water. Limnol. Oceanogr. 43, 1500–1510.

Berger, W.H., Wefer, G., 2002. On the reconstruction of upwelling history: Namibia upwelling in context. Mar. Geol. 180, 3–28.

Berner, R.A., 1980. Early Diagenesis, A Theoretical Approach. Princeton University Press, Princeton.

Biddle, J.F., Lipp, J.S., Lever, M.A., Lloyd, K.G., Sørensen, K.B., Anderson, R., Fredricks, H.F., Elvert, M., Kelly, T.J., Schrag, D.P., Sogin, M.L., Brenchley, J.E., Teske, A., House, C.H., Hinrichs, K.-U., 2006. Heterotrophic Archaea dominate sedimentary subsurface ecosystems off Peru. PNAS 104, 3846–3851.

Boetius, A., Ravenschlag, K., Schubert, C.J., Rickert, D., Widdel, F., Gieseke, A., Amann, R., Jørgensen, B.B., Witte, U., Pfannkuche, O., 2000. A marine microbial consortium apparently mediating anaerobic oxidation of methane. Nature 407, 623–626.

Boudreau, B.P., 1997. Diagenetic Models and their Implementation: Modelling Transport and Reactions in Aquatic Sediments. Springer-Verlag, Berlin. 414 pp.

Boudreau, B.P., Canfield, D.E., 1988. A Provisional Diagenetic Model for pH in Anoxic Porewaters - Application to the Foam Site. J. Mar. Res. 46, 429–455.

Boudreau, B.P., Ruddick, B.R., 1991. On a reactive continuum representation of organic-matter diagenesis. Am. J. Sci. 291, 507–538.

Burdige, D.J., 2006. Geochemistry of Marine Sediments. Princeton University Press, Princeton, 630 pp.

Canfield, D.E., 1994. Factors influencing organic carbon preservation in marine sediments. Chem. Geol. 114, 315–329.

Compton, J.S., 1988. Degree of supersaturation and precipitation of organogenic dolomite. Geology 16, 318–321.

Compton, J.S., Siever, R., 1986. Diffusion and mass balance of Mg during early dolomite formation, Monterey Formation. Geochim. Cosmochim. Acta 50, 125–135.

Coplen, T.B., Brand, W.A., Gehre, M., Groning, M., Meijer, H.A.J., Toman, B., Verkouteren, R.M., 2006. New guidelines for delta C-13 measurements. Anal. Chem. 78, 2439–2441.

D'Hondt, S., Rutherford, S., Spivack, A.J., 2002. Metabolic activity of subsurface life in deep-sea sediments. Science 295, 2067–2070.

D'Hondt, S., Jørgensen, B.B., Miller, D.J., Batzke, A., Blake, R., Cragg, B.A., Cypionka, H., Dickens, G.R., Ferdelman, T., Hinrichs, K.U., Holm, N.G., Mitterer, R., Spivack, A., Wang, G.Z., Bekins, B., Engelen, B., Ford, K., Gettemy, G., Rutherford, S.D., Sass, H., Skilbeck, C.G., Aiello, I.W., Guerin, G., House, C.H., Inagaki, F., Meister, P., Naehr, T., Niitsuma, S., Parkes, R.J., Schippers, A., Smith, D.C., Teske, A., Wiegel, J., Padilla, C.N., Acosta, J.L.S., 2004. Distributions of microbial activities in deep subseafloor sediments. Science 306, 2216–2221.

Expedition 323 Scientists, 2010. Bering Sea paleoceanography: Pliocene–Pleistocene paleoceanography and climate history of the Bering Sea. Integrated Ocean Drilling Program, Preliminary Report 323. doi:10.2204/iodp.pr.323.2010.

Ferry, J.G., 1992. Methane from acetate. J. Bacteriol. 174, 5489–5495.

Garcia, H.E., Locarnini, R.A., Boyer, T.P., Antonov, J.I., 2006. World Ocean Atlas 2005, Volume 3: Dissolved Oxygen, Apparent Oxygen Utilization, and Oxygen Saturation. In: Levitus, S. (Ed.), NOAA Atlas NESDIS 63. U.S. Government Printing Office, Washington, D.C. 342 pp.

Gieskes, J.M., Gamo, T., Brumsack, H., 1991. Chemical methods for interstitial water analysis aboard JOIDES Resolution. ODP Tech. Note 15. doi:10.2973/odp.tn.15.1991.

Hansell, D.A., Whitledge, T.E., Goering, J.J., 1993. Patterns of nitrate utilization and new production over the Bering-Chukchi Shelf. Cont. Shelf Res. 13, 601–627.

Hartnett, H.E., Devol, A.H., 2003. Role of a strong oxygen-deficient zone in the preservation and degradation of organic matter: a carbon budget for the continental margins of northwest Mexico and Washington State. Geochim. Cosmochim. Acta 67, 247–264.

Hedges, J.I., Keil, R.G., 1995. Sedimentary organic matter preservation — an assessment and speculative synthesis. Mar. Chem. 49, 81–115.

Hensen, C., Wallmann, K., 2005. Methane formation at Costa Rica continental margin-constraints for gas hydrate inventories and cross-décollement fluid flow. Earth Planet. Sci. Lett. 236, 41–60.

Hoehler, T.M., Alperin, M.J., Albert, D.B., Martens, C.S., 1994. Field and laboratory studies of methane oxidation in an anoxic marine sediment — evidence for a methanogen-sulfate reducer consortium. Glob. Biogeochem. Cycles 8, 451–463.

Johnson, G.C., Stabeno, P.J., Riser, S.C., 2004. The Bering Slope Current system revisited. J. Phys. Oceanogr. 34, 384–398.

Jørgensen, B.B., D'Hondt, S., Miller, D.J., 2006. Leg 201 synthesis: controls on microbial communities in deeply buried sediments. In: Jørgensen, B.B., D'Hondt, S., Miller, D.J. (Eds.), Proceedings of the Ocean Drilling Program, Scientific Results, 201. Ocean Drilling Program, College Station, Texas.

Jourabchi, P., Meile, C., Pasion, L.R., Van Cappellen, P., 2008. Quantitative interpretation of pore water O_2 and pH distributions in deep-sea sediments. Geochim. Cosmochim. Acta 72, 1350–1364.

Kastner, M., Torres, M., Solomon, E., Spivack, A.J., 2008. Marine pore fluid profiles of dissolved sulfate; do they reflect in situ methane fluxes ? Fire in the Ice Summer, pp. 6–8.

Kelts, K., McKenzie, J.A., 1982. Diagenetic dolomite formation in quaternary anoxic diatomaceous muds of deep-sea drilling project Leg-64, Gulf of California. Init. Rep. Deep Sea Drilling Proj. 64, 553–569. doi:10.2973/dsdp.proc.64.110.1982.

Kinder, T.H., Coachman, L.K., 1978. Front overlaying continental slope in Eastern Bering Sea. J. Geophys. Res. Oceans 83, 4551–4559.

Ladd, C., Stabeno, P.J., 2009. Freshwater transport from the Pacific to the Bering Sea through Amukta Pass. Geophys. Res. Lett. 36.

Lippmann, F., 1973. Sedimentary Carbonate Minerals. Springer-Verlag, New York, p. 228.

Luff, R., Wallmann, K., 2003. Fluid flow, methane fluxes, carbonate precipitation and biogeochemical turnover in gas hydrate-bearing sediments at Hydrate Ridge, Cascadia Margin: Numerical modeling and mass balances. Geochim. Cosmochim. Acta 67, 3403–3421.

Mackin, J.E., Aller, R.C., 1984. Ammonium adsorption in marine-sediments. Limnol. Oceanogr. 29, 250–257.

Manheim, F.T., Brooks, E.G., Winters, W.J., 1994. Description of a hydraulic sediment squeezer. U.S. Geological Survey Open-File Report 94–584. 39 pp.

Martens, C.S., Berner, R.A., 1974. Methane production in interstitial waters of Sulfate-depleted marine sediments. Science 185, 1167–1169.

Martens, C.S., Albert, D.B., Alperin, M.J., 1999. Stable isotope tracing of anaerobic methane oxidation in the gassy sediments of Eckernforde Bay, German Baltic Sea. Am. J. Sci. 299, 586–610.

Mazzullo, S.J., 2000. Organogenic dolomitization in peritidal to deep-sea sediments. J. Sed. Res. 70, 10–23.

McCorkle, D.C., Emerson, S.R., Quay, P.D., 1985. Stable carbon isotopes in marine pore-waters. Earth Planet. Sci. Lett. 74, 13–26.

Meister, P., McKenzie, J.A., Vasconcelos, C., Bernasconi, S., Frank, M., Gutjahr, M., Schrag, D.P., 2007. Dolomite formation in the dynamic deep biosphere: results from the Peru Margin. Sedimentology 54, 1007–1031.

Middelburg, J.J., 1989. A simple rate model for organic matter decomposition in marine sediments. Geochim. Cosmochim. Acta 53, 1577–1581.

Middelburg, J.J., Levin, L.A., 2009. Coastal hypoxia and sediment biogeochemistry. Biogeosciences 6, 1273–1293.

Mitterer, R.M., 2010. Methanogenesis and sulfate reduction in marine sediments: a new model. Earth Planet. Sci. Lett. 295, 358–366.

Mix, A.C., Tiedemann, R., Blum, P., et al., 2003. Proceedings of the Ocean Drilling Program, Initial Reports 202. doi:10.2973/odp.proc.ir.202.2003.

Moore, J.K., Doney, S.C., Glover, D.M., Fung, I.Y., 2002. Iron cycling and nutrient-limitation patterns in surface waters of the World Ocean. Deep-Sea Res. Pt. II 49, 463–507.

Moore, T.S., Murray, R.W., Kurtz, A.C., Schrag, D.P., 2004. Anaerobic methane oxidation and the formation of dolomite. Earth Planet. Sci. Lett. 229, 141–154.

Müller, P.J., 1977. C/N ratios in Pacific deep-sea sediments — effect of inorganic ammonium and organic nitrogen compounds sorbed by clays. Geochim. Cosmochim. Acta 41, 765–776.

Niewöhner, C., Hensen, C., Kasten, S., Zabel, M., Schulz, H.D., 1998. Deep sulfate reduction completely mediated by anaerobic methane oxidation in sediments of the upwelling area off Namibia. Geochim. Cosmochim. Acta 62, 455–464.

Okkonen, S.R., Schmidt, G.M., Cokelet, E.D., Stabeno, P.J., 2004. Satellite and hydrographic observations of the Bering Sea 'Green Belt'. Deep-Sea Res. Pt. II 51, 1033–1051.

Parkes, R.J., Webster, G., Cragg, B.A., Weightman, A.J., Newberry, C.J., Ferdelman, T.G., Kallmeyer, J., Jørgensen, B.B., Aiello, I.W., Fry, J.C., 2005. Deep sub-seafloor prokaryotes stimulated at interfaces over geological time. Nature 436, 390–394.

Paull, C.K., Lorenson, T.D., Dickens, G., Borowski, W.S., Ussler, W., Kvenvolden, K., 2000. Comparisons of in situ and core gas measurements in ODP Leg 164 bore holes, Gas Hydrates: Challenges for the Future. Ann. NY Acad. Sci. 912, 23–31.

Pimmel, A., Claypool, G., 2001. Introduction to shipboard organic geochemistry on the JOIDES Resolution. ODP Tech. Note 30. doi:10.2973/odp.tn.30.2001.

Reed, R.K., 1990. A year-long observation of water exchange between the North Pacific and the Bering Sea. Limnol. Oceanogr. 35, 1604–1609.

Sambrotto, R.N., Mordy, C., Zeeman, S.I., Stabeno, P.J., Macklin, S.A., 2008. Physical forcing and nutrient conditions associated with patterns of Chl a and phytoplank-ton productivity in the southeastern Bering Sea during summer. Deep-Sea Res. Pt. II 55, 1745–1760.

Sansone, F.J., Martens, C.S., 1981. Methane production from acetate and associated methane fluxes from anoxic coastal sediments. Science 211, 707–709.

Schippers, A., Neretin, L.N., Kallmeyer, J., Ferdelman, T.G., Cragg, B.A., Parkes, R.J., Jørgensen, B.B., 2005. Prokaryotic cells of the deep sub-seafloor biosphere identified as living bacteria. Nature 433, 861–864.

Schrum, H.N., Spivack, A.J., Kastner, M., D'Hondt, S., 2009. Sulfate-reducing denitrifi-cation: a thermodynamically feasible metabolic pathway in subseafloor sediments. Geology 37, 939–942.

Sivan, O., Schrag, D.P., Murray, R.W., 2007. Rates of methanogenesis and methanotrophy in deep-sea sediments. Geobiology 5, 141–151.

Snyder, G.T., Hiruta, A., Matsurnoto, R., Dickens, G.R., Tomaru, H., Takeuchi, R., Komatsubara, J., Ishida, Y., Yu, H., 2007. Pore water profiles and authigenic mineralization in shallow marine sediments above the methane-charged system on Umitaka Spur, Japan Sea. Deep-Sea Res. Pt. II 54, 1216–1239.

Soetaert, K., Hofmann, A.F., Middelburg, J.J., Meysman, F.J.R., Greenwood, J., 2007. The effect of biogeochemical processes on pH. Mar. Chem. 106, 380–401.

Solórzano, L., 1969. Determination of Ammonia in Natural Waters by Phenolhypochlorite Method. Limnol. Oceanogr. 14, 799–801.

Springer, A.M., McRoy, C.P., Flint, M.V., 1996. The Bering Sea Green Belt: shelf-edge processes and ecosystem production. Fish. Oceanogr. 5, 205–223.

Stabeno, P.J., Schumacher, J.D., Ohtani, K., 1999. The physical oceanography of the Bering Sea. In: Loughlin, T.R., Ohtani, K. (Eds.), Dynamics of the Bering Sea. North Pacific Marine Science Organization (PICES), Fairbanks, pp. 1–28.

Stabeno, P.J., Reed, R.K., Napp, J.M., 2002. Transport through Unimak Pass, Alaska. Deep Sea Res. Pt. II 49, 5919–5930.

Stabeno, P.J., Ladd, C., Reed, R.K., 2009. Observations of the Aleutian North Slope Current, Bering Sea, 1996–2001. J. Geophys. Res. Oceans 114, C05015.

Stumm, W., Morgan, J.J., 1996. Aquatic Chemistry: Chemical Equilibria and Rates in Natural Waters. J. Wiley & Sons, New York.

Takahashi, K., 1998. The Bering and Okhotsk Seas: modern and past paleoceanographic changes and gateway impact. J. Asian Earth Sci. 16, 49–58.

Takahashi, K., 1999. Paleoceanographic changes and present environment of the Bering Sea. In: Loughlin, T.R., Ohtani, K. (Eds.), Dynamics of the Bering Sea. North Pacific Marine Science Organization (PICES), Fairbanks, pp. 365–385.

Torres, M.E., Mix, A.C., Rugh, W.D., 2005. Precise delta C-13 analysis of dissolved inorganic carbon in natural waters using automated headspace sampling and continuous-flow mass spectrometry. Limnol. Oceanogr. Meth. 3, 349–360.

Treude, T., Niggemann, J., Kallmeyer, J., Wintersteller, P., Schubert, J.C., Boetius, A., Jørgensen, B.B., 2005. Anaerobic oxidation of methane and sulfate reduction along the Chilean continental margin. Geochim. Cosmochim. Acta 69, 2767–2779.

Tyrrell, T., Merico, A., Waniek, J.J., Wong, C.S., Metzl, N., Whitney, F., 2005. Effect of seafloor depth on phytoplankton blooms in high-nitrate, low-chlorophyll (HNLC) regions. J. Geophys. Res.-Biogeo. 110, G02007.

Ullman, W.J., Aller, R.C., 1982. Diffusion-coefficients in nearshore marine-sediments. Limnol. Oceanogr. 27, 552–556.

Ussler, W., Paull, C.K., 2008. Rates of anaerobic oxidation of methane and authigenic carbonate mineralization in methane-rich deep-sea sediments inferred from models and geochemical profiles. Earth Planet. Sci. Lett. 266, 271–287.

Valentine, D.L., Reeburgh, W.S., 2000. New perspectives on anaerobic methane oxidation. Environ. Microbiol. 2, 477–484.

Vandewiele, S., Cowie, G., Soetaert, K., Middelburg, J.J., 2009. Amino acid biogeochemistry and organic matter degradation state across the Pakistan margin oxygen minimum zone. Deep-Sea Res. Pt. II 56, 376–392.

Wallmann, K., Aloisi, G., Haeckel, M., Obzhirov, A., Pavlova, G., Tishchenko, P., 2006. Kinetics of organic matter degradation, microbial methane generation, and gas hydrate formation in anoxic marine sediments. Geochim. Cosmochim. Acta 70, 3905–3927.

Wallmann, K., Aloisi, G., Haeckel, M., Tishchenko, P., Pavlova, G., Greinert, J., Kutterolf, S., Eisenhauer, A., 2008. Silicate weathering in anoxic marine sediments. Geochim. Cosmochim. Acta 72, 3067–3090.

Wehrmann, L.M., Knab, N.J., Pirlet, H., Unnithan, V., Wild, C., Ferdelman, T.G., 2009. Carbon mineralization and carbonate preservation in modern cold-water coral reef sediments on the Norwegian shelf. Biogeosciences 6, 663–680.

Whiticar, M.J., 1999. Carbon and hydrogen isotope systematics of bacterial formation and oxidation of methane. Chem. Geol. 161, 291–314.

Whiticar, M.J., Faber, E., Schoell, M., 1986. Biogenic methane formation in marine and freshwater environments — CO$_2$ reduction *vs.* acetate fermentation-Isotope evidence. Geochim. Cosmochim. Acta 50, 693–709.